INSTITUTO DE FÍSICA

preprint

IFUSP/P-167

COMPLEX ANGULAR MOMENTUM THEORY OF THE RAINBOW AND THE GLORY

by

H. M. Nussenzveig

Instituto de Física, Universidade de São Paulo, S.P. Brazil

UNIVERSIDADE DE SÃO PAULO
INSTITUTO DE FÍSICA
Caixa Postal - 20.516
Cidade Universitária
São Paulo - BRASIL

Complex angular momentum theory of the rainbow and the glory

H. M. Nussenzveig
Instituto de Física, Universidade de São Paulo, São Paulo, Brazil

A survey is given of the applications of complex angular momentum theory to Mie scattering, with special emphasis on the recent treatments of the rainbow and the glory. The theory yields uniform asymptotic expansions of the scattering amplitudes for rainbows of arbitrary order, for size parameters $\gtrsim 50$, in close agreement with the exact results. The Airy theory fails for parallel polarization in the primary bow and for both polarizations in higher-order rainbows. The theory provides for the first time a complete physical explanation of the glory. It leads to the identification of the dominant contributions to the glory and to asymptotic expressions for them. They include a surface-wave contribution, whose relevance was first conjectured by van de Hulst, and the effect of complex rays in the shadow of the tenth-order rainbow . Good agreement with the exact results is obtained. Physic

al effects that play an important role include axial focusing, cross-polarization, orbiting, the interplay of various damping effects, and geometrical resonances associated with closed or almost-closed orbits. All significant features of the glory pattern found in recent numerical studies are reproduced.

1. INTRODUCTION

Analysing exact solutions for the diffraction of light by an object, Sommerfeld points out in his lectures on optics[1]:

"The simplest example of such an object is the sphere. The field outside a sphere can be represented by series of spherical harmonics and Bessel functions of half-integer indices. These series have been discussed by G. Mie for colloidal particles of arbitrary composi - tions. But even there a mathematical difficulty develops which quite generally is a drawback of this "method of series development": for fairly large particles ($ka > 1$, a = radius, $k = 2\pi/\lambda$) the series converge so slowly that they become practically useless. Except for this diffi- culty we could in this way obtain a complete solution of the problem of the rainbow, the difficulty of which was pointed out..."

The purpose of this review is to outline how this problem has finally been solved, through the application of complex angular momentum techniques originally introdu ced by Poincaré and Watson essentially for this purpose, and to which Sommerfeld himself gave important contribu- tions. These techniques enable us to solve not only the problem of the rainbow, "that most impressive of celestial phenomena" (in Sommerfeld's expression), but also a much more difficult one, posed by an equally beautiful, though more elusive, phenomenon: the glory. While the physical origin of the rainbow was well understood, this was not

so for the glory, although a conjectured explanation by van de Hulst[2,3] included some of the relevant effects.

The essential role played by the extension to complex variables in the solution deserves some discussion. An early example of such an extension is Sommerfeld's own solution of the half-plane diffraction problem. It would be misleading to view this extension as some contrived mathematical device: it has a much deeper significance.

We are accustomed to picturing optics in terms of real rays. It will be seen, though, that "complex rays", which represent the analytic continuation of real rays to complex values of some associated parameters, play an important role in both the rainbow and the glory.

Complex rays are already well-known in optics in total reflection, where they describe the exponentially damped penetration into the rarer medium, associated with surface waves travelling along the boundary. This typical wave effect is responsible, in quantum mechanics, for the tunneling through a potential barrier. It is very natural, from this viewpoint, to describe diffraction in terms of complex rays, since diffraction always represents the penetration of light into regions that are forbidden to the real rays of geometrical optics.

We begin with a brief survey of the complex angular momentum theory, as applied to the present problem (Sect.2). The applications to the rainbow and the glory are described in Sects. 3 and 4, respectively. The conclusions and some additional applications to meteorological optics are summed up in Sect. 5.

2. COMPLEX ANGULAR MOMENTUM THEORY OF MIE SCATTERING

The Mie solution

The exact Mie solution[4] for the scattering amplitudes when a monochromatic plane wave is incident on a homogeneous sphere of radius a and refractive index N may be written as follows:

$$S_j(\beta,\theta) = \frac{1}{2}\sum_{\ell=1}^{\infty}\left\{\left[1 - S_\ell^{(j)}(\beta)\right]t_\ell(\cos\theta) + \left[1 - S_\ell^{(i)}(\beta)\right]p_\ell(\cos\theta)\right\} \quad (i,j = 1,2;\ i\neq j), \quad (2.1)$$

where $S_1(\beta,\theta)$ and $S_2(\beta,\theta)$ are the scattering amplitudes associated with perpendicular and with parallel polarization, respectively, θ is the scattering angle and $\beta = ka$ is the size parameter.

The angular functions are defined by

$$p_\nu(\cos\theta) = \left[P_{\nu-1}(\cos\theta) - P_{\nu+1}(\cos\theta)\right]/\sin^2\theta, \quad (2.2)$$

$$t_\nu(\cos\theta) = -\cos\theta\, p_\nu(\cos\theta) + (2\nu+1)\, P_\nu(\cos\theta), \quad (2.3)$$

where $P_\nu(\cos\theta)$ is the Legendre function of the first kind (Legendre polynomial, when $\nu = \ell$ is an integer). The functions $S_\ell^{(j)}(\beta)$ are S-matrix elements associated with magnetic (j=1) and electric (j=2) multipoles of order ℓ, respectively. They are given by

$$S_\ell^{(j)}(\beta) = -\frac{\zeta_\ell^{(2)}(\beta)}{\zeta_\ell^{(1)}(\beta)}\left[\frac{\ell n'\ \zeta_\ell^{(2)}(\beta) - N\eta_j\ell n'\psi_\ell(\alpha)}{\ell n'\ \zeta_\ell^{(1)}(\beta) - N\eta_j\ell n'\psi_\ell(\alpha)}\right], \quad (2.4)$$

where

$$n_1 = 1 \quad , \quad n_2 = N^{-2} \quad , \quad \alpha = N\beta \tag{2.5}$$

and ψ_ℓ and $\zeta_\ell^{(1,2)}$ are the Ricatti-Bessel and Ricatti--Hankel functions, respectively.

The scattered intensities for the two polariza - tions are given by

$$i_j(\beta,\theta) = |S_j(\beta,\theta)|^2 \ , \tag{2.6}$$

and $\delta(\beta,\theta) = \arg S_1 - \arg S_2$ determines the state of polarization of the scattered light.

Except near $\theta = 0$ and $\theta = \pi$, the contribution from t_ℓ is dominant over that from p_ℓ in (2.1), so that S_1 (S_2) is dominated by magnetic (electric) multi- pole contributions.

In the domain of interest ($\beta >> 1$), the ℓth "partial wave" in (2.1) is associated with incident rays having an impact parameter b_ℓ given by the "localiza- tion principle"

$$b_\ell = (\ell + \tfrac{1}{2})/k \ . \tag{2.7}$$

We expect that only rays hitting the sphere ($b_\ell \leq a$) are significantly scattered, so that the number of terms that must be retained in the Mie series to get an accurate re- sult should be of the order of β . For visible light scattered by water droplets in the atmosphere, β ranges up to values of several thousand. This justifies Som - merfeld's statement quoted in Sect. 1.

Numerical calculations of backscattering[5,6] based on (2.1) have shown an extremely rapid variation of the intensity with β. To resolve the details, the computations are made at intervals $\delta\beta = 10^{-2}$, with double precision arithmetic, using 11 significant decimal digits. The intensities are also rapidly-varying functions of N and θ. Thus, even the availability of large computers has not solved the practical problem of extracting the information contained in the Mie solution.

The Watson transformation

Complex angular momentum techniques were introduced to deal with this problem in the early years of this century[7]. The Watson transformation starts by rewriting a partial-wave series such as (2.1) as a contour integral around the positive real half-axis in the λ-plane, where

$$\lambda = \ell + \frac{1}{2} \tag{2.8}$$

is now regarded as a complex variable ("complex angular momentum"), and a suitable factor is introduced to generate poles at the physical values of λ (integral ℓ), so that the corresponding residues reproduce the partial-wave series.

The advantage of rewriting the series as a path integral is that the path may be deformed in the λ-plane, and one may then look for paths such that the dominant high-frequency contributions arise from a small number of critical points, instead of being distributed among a large number of partial waves.

Watson's interest was in radio wave propagation , and he confined his attention to the deep shadow of a highly absorbing sphere (the Earth), where the critical points are complex poles, now known as Regge poles. The corresponding residues are "creeping waves"[8] generated by incident rays tangent to the sphere, and travelling around it as surface waves, rapidly damped by radiation in tangential directions. The imaginary part of the poles,which determines the damping, increases rapidly, leading to a rapidly-convergent residue series in the deep shadow region. The results can also be interpreted in terms of "diffracted rays", as shown by Keller[9] in his geometrical theory of diffraction.

In a lit region, Regge poles, as a rule, are not dominant critical points any longer. Such a region is accessible to geometrical-optic rays; since real rays correspond to stationary optical paths by Fermat's principle, they give rise to stationary-phase points on the real λ-axis. These are then real saddle points, which are the new dominant critical points, and one looks for a different deformation of the original path integral into a "background integral", so as to include portions of the associated steepest-descent paths going through the new critical points. Fock[10] was one of the main proponents [7] of this idea. He also studied the transition from light to shadow ("penumbra") on the surface of the sphere, and showed that it is described by a new mathematical function, the Fock function.

Applications of Watson's transformation to diffraction up to this point, including Fock's reformulation,were

limited in scope to only a few disconnected regions of space. It was applied to the rainbow problem by van der Pol and Bremmer[11], who employed it to recover Airy's approximation, but they did not go any further.

The modified Watson transformation

In 1965, the author[12] developed a modified form of the Watson transformation that can be applied in any region of space. For an impenetrable sphere, one starts by applying to the partial-wave series the Poisson sum formula

$$\sum_{\ell=0}^{\infty} \phi(\ell+\tfrac{1}{2}, \underset{\sim}{r}) = \sum_{m=-\infty}^{\infty} (-)^m \int_0^{\infty} \phi(\lambda, \underset{\sim}{r}) \exp(2im\pi\lambda)\, d\lambda, \qquad (2.9)$$

where the "interpolating function" $\phi(\lambda, \underset{\sim}{r})$ reduces to $\phi(\ell+\frac{1}{2}, \underset{\sim}{r})$ at the physical points. The term m=0 in (2.9) corresponds to approximating the sum by an integral[13]. Terms with $m \neq 0$ are associated with paths that wind $|m|$ times around the center of the sphere.

Making use of reflection properties of the integrand, one can rewrite (2.9) in terms of integrals over the whole real axis, which are then judiciously deformed into the complex λ-plane. Different deformations are employed in different regions of space. They usually lead to background integrals and to residues at Regge poles, with interpretations similar to those given above. Finally, one must consider the transitional domains between different spatial regions, where diffraction effects appear. We refer to a previous survey[14] for an account of this work.

The method succeeds for an impenetrable sphere because of the rapid damping of the surface waves associated with the Regge-pole contributions. This damping is determined by a purely geometrical property, the curvature of the surface, which gives rise to radiation as the waves travel around it.

The Debye expansion

If the sphere is penetrable, the waves get inside, leading to resonance effects with much weaker damping. Correspondingly, many Regge poles are located close to the real axis, spoiling the rapid convergence.

In order to recover it, the solution must be rewritten in terms of surface interactions. This can be done by a procedure similar to the multiple-reflection treatment of the Fabry-Perot interferometer[1]: each spherical multipole wave undergoes successive internal reflections from the surface and from the center of the sphere (which simulates a perfect reflector, converting incoming waves into outgoing ones). The resulting expansion was employed by Debye[15] for a cylinder, so that we call it the Debye expansion. For the $\underline{S}$-matrix elements in (2.1), it is of the form

$$S_\ell^{(j)}(\beta) = \frac{\zeta_\ell^{(2)}(\beta)}{\zeta_\ell^{(1)}(\beta)} R_{22}^{(j)} + \frac{\zeta_\ell^{(2)}(\beta)}{\zeta_\ell^{(1)}(\beta)} \frac{\zeta_\ell^{(1)}(\alpha)}{\zeta_\ell^{(2)}(\alpha)} T_{21}^{(j)} T_{12}^{(j)} \cdot$$

$$\times \left(\sum_{p=1}^{P} \rho_j^{p-1} + \frac{\rho_j^{P}}{1-\rho_j} \right), \qquad (2.10)$$

where

$$\rho_j = \left[\zeta_\ell^{(1)}(\alpha)/\zeta_\ell^{(2)}(\alpha)\right] R_{11}^{(j)} \qquad (2.11)$$

and $T_{rs}^{(j)}$, $R_{rs}^{(j)}$ $(r,s = 1,2)$ are spherical transmission and reflection coefficients between region 1 (inside the sphere) and region 2 (outside the sphere) . They are given by expressions similar to (2.4), except that they involve $\zeta_\ell^{(1,2)}(\alpha)$ instead of $\psi_\ell(\alpha)$ (i.e., travelling waves instead of standing waves inside the sphere).

The corresponding Debye expansion of (2.1) is

$$S_j(\beta,\theta) = S_{j,o}(\beta,\theta) + \sum_{p=1}^{P} S_{j,p}(\beta,\theta) + \text{remainder}, \qquad (2.12)$$

where $S_{j,o}$ is associated with direct reflection from the surface and $S_{j,p}$, the pth term of the Debye expansion , is associated with transmission after (p-1) internal reflections at the surface. Since $|\rho_j| < 1$, we can even let $P \to \infty$ in (2.10) and (2.12), but the above form yields the remainder after P terms.

We can now apply the modified Watson transformation to each term in (2.12). Since only surface interactions are involved, the corresponding poles in the λ-plane,which we call Regge-Debye poles, are all associated with rapidly-damped surface waves, so that we get rapidly-convergent asymptotic expansions for each Debye term[16].

On the other hand, $|\rho_j(\ell,\beta)|$, as defined by (2.11), is approximately equal to the Fresnel reflection coefficient at the corresponding impact parameter (2.7),which

is fairly small below the "edge domain"

$$\beta - c\beta^{1/3} \lesssim \ell \lesssim \beta + c\,\beta^{1/3}\ , \quad c = \mathcal{O}(1). \qquad (2.13)$$

Thus, when the dominant contributions to (2.12) do not come from this domain, the Debye expansion converges rapidly. For water droplets, at most values of θ , we can stop at $P = 2$ in (2.12). A conspicuous exception,as will be seen below, is the glory (neighborhood of $\theta = \pi$).

Results for penetrable sphere

For each Debye term, the critical points in the λ-plane are Regge-Debye poles and saddle points (real or complex) associated with background integrals.

A real saddle point $\bar{\lambda}$ in the range $0 \leqslant \bar{\lambda} \leqslant \beta$ for the pth Debye term corresponds to a geometrical -optic ray incident at the impact parameter $\bar{\lambda}/k$ (cf. (2.7)), that undergoes (p-1) internal reflections before emerging in the direction θ , so that the Debye expan - sion also parallels the geometrical-optic ray-tracing method. For a given p , as the impact parameter ranges from 0 to a , each domain of scattering angles may be covered one or more times by geometrically scattered rays. Thus, for each p , the domain $0 \leqslant \theta \leqslant \pi$ is subdivided into angular sectors, at the level of geometrical optics, corresponding to 0-ray (shadow) regions, 1-ray regions , 2-ray regions, etc.. Each region usually requires a dif ferent path deformation to go through the associated sad dle points.

The residues at Regge-Debye poles again correspond

to surface waves excited by tangentially incident rays. In contrast with the impenetrable sphere problem, however, these waves not only travel around the surface , but also, at each point, they may undergo critical refraction into the sphere, taking a "shortcut" through it and either undergoing "total" internal reflection at the opposite side or being critically refracted to the outside, to reemerge tangentially as surface waves. For the pth Debye term, there are p shortcuts. An illustrative example for p=2 is shown in Fig. 1.

The boundary between two different angular sectors for a given Debye term is a shadow boundary, in the sense that one or more real geometrical-optic rays disappear as we cross it. The forward and backward directions may also be regarded as special boundaries in this sense . Diffraction broadens each such boundary into a transition region, and the most interesting effects are found in such regions.

In the neighborhood of the forward direction , $0 \leq \theta \leq \beta^{-1}$, one finds the forward diffraction peak , where the intensity is dominated by the well-known Airy pattern of Fraunhofer diffraction by a circular disk.

A common transition region is associated with the disappearance of one real ray. In the λ-plane, one type of critical point, a real saddle point, is replaced by a set of Regge-Debye poles. We call the corresponding transition a Fock-type transition, because the amplitudes in the transition region are described by Fock-type functions. These functions are defined by integrals whose

asymptotic behavior is determined by a saddle point on one side of the transition and by a residue series on the other side; in between, they interpolate smoothly between the two types of behavior. The angular width of Fock-type transition regions is, typically, of the order of $\beta^{-1/3}$.

The other types of transition regions found in this problem are rainbow regions and the glory region. Their treatment, the main topic of the present review , is discussed below.

3. THE RAINBOW

Previous theories

A rainbow occurs when the scattering angle, as a function of impact parameter, goes through an extremum. The "folding back" of the corresponding scattered ray takes place at the extremal scattering angle, the rainbow angle. Thus, two rays scattered in the same direction with different impact parameters on the lit side of the rainbow fuse together at the rainbow angle and then disappear as we go over to the dark side. This is one of the simplest examples of a "fold catastrophe" in the sense of Thom[17].

Rainbows of different orders are associated with Debye terms of different orders; multiple reflection renders them fainter as their order increases. The most common rainbows are the primary bow, associated with p=2 in (2.12), and the secondary bow, associated with p = 3.

Descartes' geometrical theory of the rainbow explained the primary and secondary bows in terms of the intensity enhancements at the extremal scattering angles for $p=2$ and $p=3$, respectively; it also explained the dark band in the sky between the two bows (Fig. 2) as a shadow side common to both bows. Since a rainbow angle corresponds to a caustic for the scattered rays, geometrical optics predicts infinite intensity at a rainbow angle, as well as zero intensity on the dark side.

The supernumerary arcs (Fig. 2) were explained by Young as one of the earliest examples of interference phenomena: they arise from the interference between the two scattered rays on the lit side which merge together at the rainbow angle.

Classical diffraction theory was applied to the rainbow by Airy[18]. He applied the Huygens-Fresnel principle to a virtual wave front associated with geometrically scattered rays near the rainbow angle, making an assumption similar to Kirchhoff's approximation: constant amplitude along this wave front. The result was his celebrated "rainbow integral", now known as the Airy function, which plays in rainbow phenomena a role similar to that of Fresnel's integral in Fresnel diffraction. It shows oscillatory behavior on the lit side, corresponding to the supernumerary arcs, and it is damped out faster than exponentially on the dark side.

Light from the rainbow is strongly polarized perpendicular to the observation plane, as was discovered by Biot and Brewster. The suppression of the parallel com -

ponent is due to a coincidence: the angle of incidence, for the primary bow, is close to Brewster's angle. A more detailed survey of the historical development of the theory of the rainbow can be found elsewhere[19].

The domain of validity of Airy's theory was investigated by van de Hulst[3], who concluded that it is limited, by the constant-amplitude assumption, to $\beta \geq 5{,}000$ and to $|\varepsilon| \leq 0.5^{o}$, where

$$\varepsilon = \theta - \theta_R \tag{3.1}$$

is the deviation from the rainbow angle θ_R. He pointed out at the time that no quantitative rainbow theory was available outside of this domain (apart from the numerical summation of the Mie series).

Complex angular momentum theory of the rainbow

The complex angular momentum theory allows us to derive the asymptotic behavior of the exact Mie solution in a rainbow region[20,21], bridging the gap towards lower values of β and larger $|\varepsilon|$.

For a Debye term of given order p, a rainbow is characterized, in the λ-plane, by the occurrence of two real saddle points $\bar{\lambda}'$ and $\bar{\lambda}''$ between 0 and β in some domain of scattering angles θ, corresponding to the two scattered rays on the lit side. When θ approaches θ_R from this side, the two saddle points move towards each other along the real axis, merging together at $\theta = \theta_R$. As θ goes over to the dark side, the two saddle

points become complex, moving away from the real axis along complex conjugate directions. Thus, from a mathematical point of view, a rainbow can be defined as a collision between two saddle points in the complex angular momentum plane (Fig. 3).

It is well-known in the saddle-point method that each saddle point has a characteristic range, the region of the complex plane around it which yields the main contribution to the integral. Within the rainbow region, the ranges of the saddle points $\overline{\lambda}'$ and $\overline{\lambda}''$ overlap, so that the usual method cannot be applied.

Uniform asymptotic expansions of integrals with overlapping saddle points were first derived by Chester, Friedman and Ursell[22].

According to (2.7) and (2.8) and to the relation $b = a \sin\theta_1$ between the impact parameter b and the angle of incidence θ_1, the saddle points $\overline{\lambda}'$ and $\overline{\lambda}''$ may be written as

$$\overline{\lambda}' = \beta\sin\theta'_1 = N\beta\sin\theta'_2; \quad \overline{\lambda}'' = \beta\sin\theta''_1 = N\beta\sin\theta''_2, \qquad (3.2)$$

where, on the lit side, θ'_1 and θ''_1 are the angles of incidence of the two scattered rays that merge at the rainbow angle (θ'_2 and θ''_2 are the corresponding angles of refraction); on the shadow side, θ'_1 and θ''_1 become complex.

The angle of incidence $\theta_{1R,p}$ associated with the rainbow of order p-1 (in the pth Debye term) is given

by

$$\sin \theta_{1R,p} = (p^2 - N^2)^{1/2}/(p^2 - 1)^{1/2} \quad (p = 2,3,\ldots), \tag{3.3}$$

and θ'_1 and θ''_1 may be regarded as functions of ε, where ε is given by (3.1), with θ_R now referring to the pth term.

The Chester-Friedman-Ursell method leads to expressions of the following form for $S_{j,p}^{(R)}$, the rainbow contribution to the pth term in (2.12) :

$$\begin{aligned} S_{j,p}^{(R)}(\beta,\varepsilon) = \beta^{7/6} \exp\left[2\beta A_p(\varepsilon)\right] . \\ \times \left\{ c_{j,p}(\beta,\varepsilon)\, \mathrm{Ai}\left[(2\beta)^{2/3}\zeta_p(\varepsilon)\right] \right. \\ \left. + d_{j,p}(\beta,\varepsilon)\, \beta^{-1/3}\, \mathrm{Ai}'\left[(2\beta)^{2/3}\zeta_p(\varepsilon)\right]\right\} , \end{aligned} \tag{3.4}$$

where $\mathrm{Ai}(z)$ is the Airy function,

$$\left\{ \begin{matrix} A_p(\varepsilon) \\ \frac{2}{3}\left[\zeta_p(\varepsilon)\right]^{3/2} \end{matrix} \right\} = \frac{i}{2}\left[pN(\cos\theta'_2 \pm \cos\theta''_2) - (\cos\theta'_1 \pm \cos\theta''_1)\right], \tag{3.5}$$

and

$$\begin{aligned} c_{j,p}(\beta,\varepsilon) &= c_{j,p}^{(0)}(\varepsilon) + \beta^{-1} c_{j,p}^{(1)}(\varepsilon) + \ldots \\ d_{j,p}(\beta,\varepsilon) &= d_{j,p}^{(0)}(\varepsilon) + \beta^{-1} d_{j,p}^{(1)}(\varepsilon) + \ldots \end{aligned} \tag{3.6}$$

are asymptotic expansions in inverse powers of β .

The r.h.s. of (3.5) is proportional to the sum (difference) of the optical paths through the sphere associated with the rays corresponding to θ'_1 and θ''_1 . The difference

vanishes at the rainbow angle: $\zeta_p(0) = 0$.

The coefficients $c_{j,p}^{(k)}$ and $d_{j,p}^{(k)}$ in (3.6) are given by expressions involving the Fresnel transmission and reflection coefficients (including multiple reflections) and their derivatives of various orders with respect to the angle of incidence, evaluated at θ_1' and θ_1'' . For small enough $|\varepsilon|$, these coefficients, as well as the functions $A_p(\varepsilon)$ and $\zeta_p(\varepsilon)$, can be expanded as power series in ε ; in particular, $\zeta_p(\varepsilon) = \theta(\varepsilon)$ for small $|\varepsilon|$.

The Airy theory corresponds to the lowest-order approximation to (3.4) in several senses: (a) $A_p(\varepsilon)$ and $\zeta_p(\varepsilon)$ are replaced by terms up to $\theta(\varepsilon)$ of their power-series expansion in ε ; (b) all coefficients $d_{j,p}^{(k)}$ are set equal to zero, so that the Ai' correction in (3.4) is neglected; (c) all coefficients $c_{j,p}^{(k)}$ for $k \geqslant 1$ are set equal to zero; (d) $c_{j,p}^{(o)}(\varepsilon)$ is approximated by $c_{j,p}^{(o)}(0)$.

Predictions of complex angular momentum theory

Let us now discuss the main features predicted by the complex angular momentum result (3.4) and compare them with previous theories.

(i) Geometrical-optic contributions to the scattering amplitudes are, typically, of order β , whereas (3.4) reaches values of order $\beta^{7/6}$ near the rainbow angle. Thus, the maximum rainbow enhancement for the amplitudes is, typically[23], of order $\beta^{1/6}$.

(ii) The main rainbow peak is characterized by $(2\beta)^{2/3}|\zeta_p(\varepsilon)| \leq 1$, where $\zeta_p(\varepsilon) = \theta(\varepsilon)$; its width ,

therefore, is $\mathcal{O}(\beta^{-2/3})$. As a function of p, the width increases [24], growing linearly with p for $p >> 1$, so that the peak becomes flatter as the order of the rainbow increases.

(iii) Within the main rainbow peak, the Ai and Ai' functions in (3.4) are of the same order, so that the dominant contribution would be expected to come from $c_{jp}^{(o)}$ in (3.6). However, $c_{jp}^{(o)}$ is proportional to the Fresnel reflection coefficient for polarization j at angles of incidence near $\theta_{1R,p}$. For the primary bow ($p=2$), $\theta_{1R,2}$ is close to Brewster's angle, so that $c_{22}^{(o)}$ is very small, rendering the Ai' correction to Airy's theory much more important for polarization 2 (parallel). The smallness of $c_{22}^{(o)}$ as compared with $c_{12}^{(o)}$ also accounts for the strong perpendicular polarization of the primary bow. Since the Fresnel reflection coefficient is always larger for perpendicular polarization, we may expect this polarization to be dominant also for higher-order rainbows.

(iv) Since $Ai'(z) / Ai(z) = \mathcal{O}(z^{1/2})$ for $|z| >> 1$, the Ai' terms become of the same order as the Ai terms in (3.4) outside of the main rainbow peak. Thus, the validity of the Airy theory is limited, at best, to small values of $|\varepsilon|$, within the main peak, in agreement with van de Hulst's criticism. For the primary bow, the worst disagreement should be found for parallel polarization: due to the dominance of the Ai' term, (3.4) predicts supernumerary peaks where the Airy theory predicts zeros, and minima at the peaks of the Airy theory. Thus, maxima and minima are interchanged for the two po

larizations. This effect, which has been observed by Bricard [25] at large angles, is related to the change of sign in the reflection coefficient as it goes through the zero at Brewster's angle. This affects one of the two scattered rays that interfere at large angles, leading to destructive rather than constructive interference.

(v) The result (3.4), in contrast with Airy's theory, is a uniform asymptotic expansion. Thus, for large $|\varepsilon|$ on the lit side, where the two real saddle points are outside each other's range, it goes over smoothly into the sum of their contributions, yielding the interference between real scattered rays that gives rise to the supernumeraries (oscillatory behavior of the Airy function).

On the shadow side, for large $|\varepsilon|$, we may employ the asymptotic expansion of Ai (z) for large positive z,

$$\mathrm{Ai}(z) \simeq z^{-1/4}\exp(-\tfrac{2}{3} z^{3/2})/2\sqrt{\pi} \quad (z >>1). \quad (3.7)$$

Although both complex saddle points contribute to (3.5) and (3.6), only the contribution from the saddle point in the lower half of the λ - plane survives for large $|\varepsilon|$, in agreement with the prediction of the steepest-descents method. Thus, (3.4) also merges smoothly with the wide-angle result on the dark side of the rainbow. This is a typical complex-ray contribution on the shadow side of a caustic[9], similar to the quantum barrier-penetration effect.

(vi) Rainbows of order higher than the second are usually masked by background glare in the sky, although

they can be observed in the laboratory [26]. While their intensity becomes progressively damped by multiple reflections, the damping weakens as the order increases, because, by (3.3), they are formed by rays closer and closer to glancing incidence. On the other hand, they become progressively broader.

The fact that high-order rainbows are formed by rays incident close to the edge has another consequence: since the Fresnel reflection coefficients are not only close to unity but also vary rapidly with the angle in this region, their derivatives with respect to angle become larger, thus enhancing the contribution of higher-order coefficients in (3.6). Therefore, the Airy approximation becomes progressively worse (for both polarizations) for higher-order rainbows.

For a rainbow formed near the backward direction, there is an additional enhancement factor arising from axial focusing, as will be seen in Sect. 4. We will see that light diffracted into the shadow of the tenth-order rainbow contributes significantly to the glory, exemplifying a (rather indirect) natural manifestation of a higher-order rainbow.

Comparison with the exact solution

Numerical comparisons between (3.4) and the exact Mie solution (2.1), as well as with the Airy approximation, have been carried out [21, 27, 28] for $N = 1.33$, $50 \leq \beta \leq 1500$, for the primary rainbow $p = 2$ ...

($136^{0} \lesssim \theta \lesssim 142^{0}$), and also, in connection with the glory [27-29], for the tenth-order rainbow (p=11). The results agree with the above predictions in all cases.

In a rainbow region, (3.4) should be the dominant contribution to the scattering amplitudes. However, to carry out comparisons with (2.1), one must take into account the effect of other Debye terms that may still yield significant (though smaller)contributions. For the primary bow, besides the rainbow term (3.4) with p = 2, one should also include the direct reflection term $S_{j,0}$ in (2.12). Its interference with the rainbow term gives rise to fast, small-amplitude oscillations superimposed on the rainbow oscillations.

As an illustration of the results, we show in Fig. 4 a comparison of the Mie, Airy and complex angular momentum results for β = 1500 and parallel polarization. To avoid the rapid oscillations, we have subtracted out the direct reflection term from the Mie solution, comparing $|S_2 - S_{2,0}|^2$, where S_2 is given by (2.1), with $|S_{2,2}^{(R)}|^2$ given by (3.4) and with the Airy approximation. In agreement with the above discussion, the Airy approximation fails badly for this polarization, except in a small neighborhood of the main rainbow peak; its out-of-phase character in the supernumeraries is apparent. The complex angular momentum result for the rainbow term agrees closely with the exact result. The deviations, which have an oscillatory character, are due to interference with higher-order Debye terms, the effects

of which will be discussed in connection with the glory.

The complex angular momentum theory, in contrast with the Airy approximation, is also in excellent agreement[21] with the exact Mie results for the phase difference $\delta = \arg S_1 - \arg S_2$. Its domain of applicability extends down to values of β of the order of 50.

4. THE GLORY

The van de Hulst conjecture

Although it offers a display hardly less impressive than the rainbow, the glory has remained a considerably more recondite phenomenon, ever since its first reported observation[30] in 1735. Its sighting (Fig. 5) requires locating the antisolar point, usually through the shadow of some object on the clouds (most often an airplane). Typical sightings occur over thin clouds or mist, with size parameters ranging from the order of a hundred to about one thousand (the average β in reported observations[3] is ~160). The intensity decrease is slower than in coronae, so that as many as five sets of colored rings have been seen. There is considerable variability in the observations; some observers have reported finding parallel polarization in the rings.

The first significant theoretical contribution towards the explanation of the glory is due to van de Hulst[2,3]. Central or near-central rays, backscattered by direct reflection or after undergoing one or more in-

ternal reflections, cannot provide an explanation: they do not lead to an intensity enhancement and their contribution is much weaker than the observed effects. Suppose, however, that a non-paraxial incident ray were to emerge in the backward direction, e.g., after one internal reflection (p=2). Such a ray is usually called a "glory ray". It was pointed out by van de Hulst that there would indeed be an intensity enhancement associated with a glory ray.

This enhancement arises from the axial symmetry. A narrow pencil of scattered rays emerging in a non-axial direction is usually associated with a virtual focus and with a portion of a spherical wave front. For a pencil of non-paraxial rays scattered in an axial direction, however, the axial symmetry spreads out the virtual focal point into a virtual focal circle,corresponding to toroidal wave fronts. Constructive interference along the axis of the rays emanating from this focal circle produces the enhancement. We will call this the axial focusing effect.

Another peculiarity of the axial direction is that the associated scattering plane is undefined. In other directions, as was noted following (2.6), the scattering amplitude for magnetic (electric) polarization is dominated by magnetic (electric) contributions, but both become comparable in the axial direction, simulating an interference between parallel and perpendicular polarization (contributions from orthogonally situated points of the virtual focal circle). This effect was also pointed

out by van de Hulst, who called it the cross-polarization effect.

For $p=2$, however, there are no glory rays, except for refractive indices in the range $\sqrt{2} < N < 2$. For the refractive index of water, the closest approach to such a ray is provided by a tangentially incident ray, which, after one internal reflection, emerges some 15^{o} away from the backward direction. It was conjectured by van de Hulst that this angular gap may be bridged by surface waves , taking paths similar to that shown in Fig. 1. We will call the effective contribution of all such paths the van de Hulst contribution.

The asymptotic evaluation of this contribution was not at hand at the time when van de Hulst formulated his conjecture, so that, although it seemed to account for some qualitative features of the glory then known, a quantitative test was missing.

Glory features revealed by numerical studies

More recently, several new numerical studies of the Mie series in the glory region have been made, revealing a remarkable degree of complexity and bringing out many new features to be explained.

Bryant and coworkers[5,31] computed the back-scattered intensity for $200.0 \leq \beta \leq 201.8$ and $500 \leq \beta \leq 501$ with $N = 1.333$, and for $3000.0 \leq \beta \leq 3001.4$, with $N = 1.333$ and $N = 1.333 + 2\times10^{-6}i$. Dave[32] computed the scattered intensity and the degree of polarization for

natural incident light as a function of θ near 180^{o}, with $N = 1.342$, for $\beta = 98.2$, 196.3, 392.7 and 785.4. Shipley and Weinman[6] computed the normalized phase function

$$P(N,\beta,\theta) = 2\beta^{-2}[i_1(N,\beta,\theta) + i_2(N,\beta,\theta)]/Q_{sca}(N,\beta) \quad , \quad (4.1)$$

where Q_{sca} is the total scattering efficiency[3], with $N=1.333$ and $\theta = \pi$, for several size parameter ranges in the interval $200 \leqslant \beta \leqslant 4520$. They also evaluated average values of (4.1) over certain ranges of size parameters. Such averages are needed in lidar (laser radar) studies of rainfall, where the droplet populations are polydisperse.

The following features of glory scattering have emerged from these numerical studies:

(i) The scattered intensities in the glory region are rapidly-varying functions of β,θ and N. Within the usual range of observation of natural glories, they are, typically, about one order of magnitude larger than the geometrical-optic axial-ray contributions.

(ii) As a function of β, the backscattered intensity shows extremely rapid quasi-periodic oscillations. For refractive indices in the range associated with water, the quasi-period $\Delta\beta$ of these oscillations ranges from about 0.81 to about 0.83.

These oscillations have been experimentally observed by Fahlen and Bryant[31] in laser light backscattered by a single water droplet, with β in the range 10^3 to 10^4: continuous evaporation of the droplet produced the variation in β. Similar observations, with β

ranging from about 50 to about 300, have been made by Saunders[33].

(iii) Within a single quasi-period, there are rapid intensity fluctuations superimposed on a relatively slowly-varying "background". The latter goes through two to three humps per quasi-period.

(iv) The rapid fluctuations include spikes where the intensity varies by one to two orders of magnitude for size parameter variations $\delta\beta \sim 0.01$ (corresponding to a change in average droplet radius of a few thousandths of a wavelength, i.e., of atomic dimensions!).

(v) The inclusion of a small absorptive term in the refractive index tends to smooth down the sharp spikes, but not the humps.

(vi) Fourier analysis of the backscattered intensity as a function of β reveals, besides the basic quasi-period, strong periodic components with the periods $\Delta_1 \beta \simeq 0.41$, $\Delta_2 \beta \simeq 1.1$ and $\Delta_3 \beta \simeq 14$ (for $N = 1.333$).

(vii) A plot of the normalized backscattering phase function, with $N = 1.333$, averaged over the largest period $\Delta_3 \beta \simeq 14$, as a function of β, in the range $200 \leqslant \beta \leqslant 4520$, shows a broad peak, with the maximum average backscattering located around $\beta \sim 10^3$.

(viii) The angular distribution and polarization of the scattered intensity for $10^2 \lesssim \beta \lesssim 10^3$ vary considerably with β. For $\beta \sim 10^2$, the first dark ring is rather hazy and the outer rings are predominantly

parallel-polarized. For $\beta \sim 10^3$, they tend to become perpendicular-polarized.

(ix) Studies[5] of numerical convergence of the Mie series show that the dominant contributions to the intensity in the glory region arise from the "edge domain" (2.13).

General considerations

The complex angular momentum theory of the glory[20,27-29,34] explains all of the above features. Let us first consider some general features of near-backward scattering.

As was mentioned following (2.6), the terms in t_ℓ in (2.1) are dominant in non-paraxial directions; on the other hand, for $\theta = \pi$, since $t_\ell(-1) = -p_\ell(-1)$, we get

$$S_1(\beta,\pi) = S^M(\beta) + S^E(\beta) = - S_2(\beta,\pi) , \qquad (4.2)$$

where S^M and S^E, the magnetic and electric contributions, are comparable, so that their interference has to be taken into account. This is van de Hulst's cross - polarization effect.

The axial focusing effect may be discussed in terms of the behavior of the angular functions (2.2) and (2.3), where $\nu = \lambda - \frac{1}{2}$. For non-paraxial ray contributions, we have $\lambda = \theta'(\beta)$, so that we may employ the asymptotic expansion of these functions for large index. For scattering angles not very close to axial directions, this introduces an extra factor $\theta'(\lambda^{-1/2}) = \theta'(\beta^{-1/2})$, as

compared with the neighborhood of axial directions. Thus, the amplitude enhancement associated with axial focusing is $\mathcal{O}(\beta^{1/2})$.

Let us concentrate our attention on the exact back scattering direction, $\theta = \pi$. The axial ray contributions arise from saddle points at $\lambda = 0$ in the even-order terms of the Debye expansion. They are readily evaluated, yielding the geometrical-optic result (plus higher-order WKB corrections). The main contributions are those from $p = 0$ and $p = 2$,

$$S_j^{axial}(\beta,\pi) \simeq S_{j,o}^{(g)}(\beta,\pi) + S_{j,2}^{(g)}(\beta,\pi) , \qquad (4.3)$$

where the superscript (g) stands for "geometrical". Higher-order axial Debye contributions are strongly damped by multiple internal reflections. The contributions (4.3) are of the form $a_j\beta$, where $|a_j|$ is of the order of the Fresnel reflection coefficient at perpendicular incidence. As was mentioned above, they are completely unable to account for the glory. They provide a smoothly-varying background, representing only a small fraction of the glory intensity.

Analysing the Debye expansion, we find that only the edge domain (2.13) can yield contributions capable of explaining the glory. This agrees with feature (ix) above. In this domain, the magnitude of the spherical reflection amplitude (2.11) is

$$|\rho_j| = |R_{11}^{(j)}| = 1 - b_j\,\beta^{-1/3} , \qquad (4.4)$$

where b_j is of the order unity; total reflection is not

reached, due to the surface curvature.

The reflection damping factor associated with the $(p+1)$th Debye term in the edge domain, for large p, is therefore

$$|\rho_j|^p \simeq \exp(-\, p\, b_j\, \beta^{-1/3}) , \qquad (4.5)$$

so that Debye terms of order up to $\mathcal{O}(\beta^{1/3})$ can still give appreciable contributions. Thus, for incident rays in the edge domain, an effect similar to "orbiting"[13] takes place. Higher-order contributions from outside of the edge domain are damped out by multiple reflections and may be neglected.

Classification of leading Debye contributions

The basic problem, when so many Debye terms may contribute, is to find out which are the leading ones and to classify them in order of decreasing importance.

In view of the axial focusing effect, it should be expected that one significant contribution would be that of a glory ray. Although such a ray does not exist for $p=2$ in water, it may exist (at least to a close approximation) for higher p, although very high values of p, for a given β, are excluded by the reflection damping factor (4.5). If

$$N = [\cos(11\pi/48)]^{-1} \simeq 1.33007 , \qquad (4.6)$$

there exists a glory ray for $p=24$. It is associated with a tangentially incident ray, which produces the closed orbit shown in Fig. 6, a regular stellated polygon

of 48 sides.

The discussion could equally well be carried out for neighboring values of N , associated with nearly-closed orbits around this or other values of p . However, it is somewhat simpler to illustrate the various effects for a value of N such that a closed orbit exists, so that we now fix N at the value (4.6). Closed or nearly-closed orbits lead to "geometrical resonance effects"[20], implying quasi-periodic features which, as we have seen, are indeed manifested in the glory.

Apart from the glory ray contribution, what other contributions from the edge domain do we expect to be important at $\theta = \pi$? We know that the edge rays give rise to surface waves with p shortcuts for the pth Debye term and that, for p=2 (van de Hulst term), the "missing angle" ζ_2 that must be described along the surface before emerging in the backward direction after two shortcuts is small (Fig. 1; $\zeta_2 = \pi/24$ for N given by (4.6)). The angular damping exponent of the surface waves, given by the imaginary part of the Regge-Debye poles, is $\mathcal{O}(\beta^{1/3})$ (cf. (4.10) below), so that, for the range of β relevant to the glory, the damping along the missing angle is not very large. Furthermore, this damping is counteracted by the enhancement due to axial focusing.

We expect, therefore, that the van de Hulst term is indeed significant. This was first quantitatively confirmed[20] for scalar scattering; however, it was also pointed out that the van de Hulst term alone cannot ac - count for the glory; there must be other significant con

tributions from higher-order Debye terms.

If the radiation damping associated with surface-wave propagation were the only damping effect, the magnitude of surface-wave contributions of order p would decrease roughly exponentially with the increase of the associated missing angle ζ_p. Restricting ourselves to surface waves that emerge less than one shortcut away from $\theta = \pi$, the angle ζ_p is given by

$$\zeta_p \equiv \pi - p\,\theta_t \pmod{2\pi},\quad 0 \leq \zeta_p < \theta_t = 2\cos^{-1}(1/N). \qquad (4.7)$$

These considerations lead to the "naive" ordering of surface-wave contributions illustrated in Fig. 6 by the decreasing length of the arrows that point at increasing values of ζ_p. Besides the values of p shown in Fig. 6, we would get additional solutions of (4.7) by adding to each p multiples of the basic period $\Delta p = 48$.

The true ordering will be affected by the reflection damping, which, according to (4.5), increases exponentially with p for high p. This cuts off higher values of p, and the cutoff point decreases when β decreases, so that this effect is of special importance within the range of β relevant to the glory. For instance, while the contributions from p=24 and $p = 37$ should be dominant over the van de Hulst p=2 term for large β, the reverse should be true for lower β.

Besides these surface-wave contributions, the edge domain also generates higher-order rainbows (cf. Sect. 3, (vi), some of which lie close to the backward direction, turning their dark side towards it. Let

$\theta_{R,p}$ denote the rainbow scattering angle for the pth Debye term. Then, the angular distance from the rainbow angle to the backward direction, for large p , is given by

$$\varepsilon_{R,p} = \pi - \theta_{R,p} \approx |\zeta_p| - (N^2-1)^{1/2}/p \quad (p>> 1) , \tag{4.8}$$

where ζ_p is defined by (4.7), now extended to negative angles.

The penetration of light within the dark side of the rainbow is described by a complex ray (Sect. 3), with a damping exponent which, for large p , according to (3.4) and (3.7), is proportional to $\beta(\varepsilon_{R,p}/p)^{3/2}$ at $\theta = \pi$. Although this is faster than the surface-wave damping, these contributions are enhanced not only by the axial focusing factor $O(\beta^{1/2})$, but also by the rainbow enhancement $O(\beta^{1/6})$.

Thus, we also expect significant contributions to the glory from complex rays on the shadow side of higher-order rainbows formed at angular distances from $\theta = \pi$ given by (4.8), for values of p such that

$$\zeta_p \equiv \pi - p\theta_t \pmod{2\pi}, \quad -\theta_t \leqslant \zeta_p < 0 . \tag{4.9}$$

The "naive" ordering of these contributions classifies them in order of decreasing importance according to increasing values of $\varepsilon_{R,p}/p$. The arrows in Fig. 6 point at the directions ζ_p , and their lengths decrease according to this "naive" ordering. The leading contribution arises from the 10th-order rainbow, for which $\varepsilon_{R,11} \approx 0.05$ rad $\approx 3^o$.

Again, the true ordering will be affected by reflection damping, the more strongly the lower the value of β. Thus, for low β, $p = 33$ should dominate over $p = 46$, while the reverse should be true for large β.

An additional consideration that affects the ordering is that the width of the main rainbow peak is $\Theta(p\,\beta^{-2/3})$ for large p (Sect. 3, (ii)), so that, for a given p, the backward direction, while lying deep within the rainbow shadow for high β, may lie within the main rainbow peak for low β, thus yielding a larger contribution, because the damping given by (3.7) has not yet set in.

Verification

To check the validity of the above discussion, the contributions from different Debye terms to $|S^M(\beta)|^2$ and $|S^E(\beta)|^2$ in (4.2) were numerically evaluated[29,34] by summing the corresponding partial-wave series for $\beta = 150$, 500 and 1,500. The results, including all terms that contribute up to ~ 0.1% to the total, are shown in Fig. 7. They are in complete agreement with our expectations.

For $\beta = 150$, which is close to the average size parameter in reported observations of the glory[3], the van de Hulst term is the leading one, followed by the 10th-order rainbow term. The two contributions become comparable at $\beta = 500$, and the 10th-order rainbow predominates at $\beta = 1{,}500$, where the glory-ray contribution ($p=24$) is already larger than the van de Hulst term for magnetic polarization.

In order to carry out a quantitative comparison with the exact Mie solution, as well as to justify the physical interpretation ascribed to the various terms in the above discussion, we must be able to asymptotically evaluate the leading Debye contributions.

For the $p = 11$ rainbow term, the complex angular momentum theory leads to an expression of the type (3.4), except that the $\mathcal{O}(\beta^{1/2})$ axial focusing enhancement replaces the factor $\beta^{7/6}$ by $\beta^{5/3}$. This should be compared with the geometrical-optic axial-ray contributions (4.3), which are $\mathcal{O}(\beta)$. The evaluation of the coefficients (3.6) shows, in agreement with our expectations (Sect. 3, (vi)), that the Airy theory fails for both polarizations at this higher value of p. A numerical comparison of the complex angular momentum prediction with the exact Mie result for the 11th Debye term [27-29,34] shows good agreement in both amplitude and phase, justifying the interpretation of this term as a complex-ray contribution on the dark side of the 10th-order rainbow. This is also a good test of the complex-angular momentum theory of the rainbow for a high-order rainbow.

For the $p = 2$ van de Hulst term, we must, according to the complex angular momentum theory, evaluate a series of residues at the Regge-Debye poles, which are of the third order for this term[20,27]. The evaluation leads to an expression of the form

$$S_{j,2}^{(res)}(\beta,\pi) = \beta^{4/3} \sum_n r_{nj} \exp(i\lambda_{nj} \zeta_2) \cdot \times \left[1 + c_{nj} \beta^{-2/3} + \mathcal{O}(\beta^{-1})\right], \tag{4.10}$$

where ζ_2 is the missing angle (4.7) for p = 2, and λ_{nj} is the nth Regge-Debye pole for polarization j, in order of increasing imaginary part; Im $\lambda_{nj} = \mathcal{O}(\beta^{1/3})$ yields the radiation damping of the surface waves.

Since Im λ_{nj} increases rapidly with n, the residue series is rapidly convergent, and it usually suffices, in practice, to keep only one or two poles. The coefficients r_{nj} are proportional to ζ_2, and therefore small, so that the $\mathcal{O}(\beta^{-2/3})$ correction inside the square brackets in (4.10) is important, specially for low β. Again, a numerical comparison with the exact Mie result[28] shows good agreement in amplitude and phase.

The asymptotic evaluation of the p = 24 glory-ray contribution is somewhat more complicated[27,34], because $\theta = \pi$ lies within a Fock transition region for this term. Numerically, the results again compare favorably with the exact Mie solution[29,34].

Complex angular momentum theory of the glory

Having at hand both the classification of the dominant Debye terms and asymptotic expressions for the leading contributions, we can finally discuss the explanation of the characteristic features of the glory listed before.

The glory arises from the interference among Debye terms of various different orders, whose relative importance varies with β. The phase factors relevant to the interference pattern originate mainly from the shortcuts through the sphere. Each shortcut contributes $2(N^2-1)^{1/2}\beta$

to the phase. With N given by (4.6), a change in β by an amount

$$\Delta\beta = 5\pi/(22\sqrt{N^2-1}) \approx 0.814 \qquad (4.11)$$

changes the phase of the dominant Debye terms in Fig. 7 either by π or by an amount close to π (mod 2π), thus leaving the intensity almost (but not quite) invariant. This explains the quasi-periodicity of the backscattered intensity, as well as the observed value of the quasi-period (feature (ii) above).

Within a quasi-period, one can consider, as a first approximation to the amplitudes, the sum of the two leading Debye terms in Fig. 7, one of which is a surface-wave term and the other a rainbow term. Comparing the resulting approximation to $|S^M(\beta)|^2$ with the exact results near β = 150, 500 and 1500, one finds[29,34] that the approximation yields the relatively slowly-varying "background", with two to three humps per quasi-period, which accounts for most of the average intensity in the glory (feature (iii)). Fig. 8 illustrates this near β = 1500.

If one includes the contributions from all the values of p shown in Fig. 6, without summing over the period $\Delta p = 48$, the result is very close to the exact curve, failing to reproduce only the sharp spikes (Fig.8).

The spikes are obtained when we carry out the summation over $\Delta p = 48$. This is illustrated for one spike by the inset in Fig. 8. Thus, the spikes represent geometrical resonance effects associated with the existence of quasi-periodic orbits. Their sharpness arises from

their association with very long optical paths with low damping (feature (iv)). If one includes a small amount of absorption, they must therefore be the first to disappear (feature (v)).

The spikes, as well as other peaks, occur at different values of β for S^M and S^E. The cross-polarization effect (interference between S^M and S^E in the backscattered intensity (4.2)) therefore gives rise to additional interference features in the total intensity.

Within the range $10^2 \lesssim \beta \lesssim 10^3$ that is most relevant to observations of the glory, the dominant contributions arise from the van de Hulst term (4.10), from the 10th-order rainbow term (given by (3.4) for $p = 11$ with an extra axial focusing factor $\beta^{1/2}$), and from the geometrical-optic axial-ray contributions (4.3):

$$S_j \approx S_{j,2}^{(res)} + S_{j,11}^{(R)} + S_{j,o}^{(g)} + S_{j,2}^{(g)} \quad (4.12)$$

In the intensity $|S_j|^2$, the interference among the terms in (4.12) gives rise to oscillations (whose amplitudes are slowly-varying on the scale of the basic quasi-period (4.11)), with quasi-periods given by: $\Delta_1\beta \simeq 0.41$ (interference between $S_{j,2}^{(res)}$ and $S_{j,11}^{(R)}$), $\Delta_2\beta \simeq 1.1$ (interference between $S_{j,2}^{(res)}$ and $S_{j,o}^{(g)}$) and $\Delta_3\beta \simeq 14$ (interference between $S_{j,2}^{(res)}$ and $S_{j,2}^{(g)}$); the quasi-periods $\Delta_2\beta$ and $\Delta_3\beta$ had already been predicted earlier[20]. These results are in complete agreement with feature (vi).

If we average $|S_j|^2$, as given by the approximation

(4.12), over the largest period $\Delta_3\beta$, we find the sum of the squared moduli of the four terms in (4.12). The last two (geometrical-optic) terms contribute only a small constant background to the average normalized phase function. The van de Hulst term (4.10) yields a contribution of order $\beta^{2/3} \exp(- c \beta^{1/3})$ (where c is of order unity). This is the leading term for $\beta \sim 10^2$, but it decreases as β increases, and is surpassed by the 10th-order rainbow contribution at values of β of the order of a few hundred. This contribution to the phase function contains a factor $\beta^{4/3}$ and terms proportional to Ai^2 and Ai'^2 (cf.(3.4)) with rather small coefficients. Due to the effect of increased width for higher-order rainbows discussed above, the backward direction falls within the main peak of the tenth-order rainbow up to $\beta \gtrsim 10^3$; thereafter, it starts to get deep within the rainbow shadow , where the strong complex-ray attenuation appears. This explains[28] why the average backscattering phase function goes through a peak around $\beta \sim 10^3$ (feature (vii)). The four-term approximation (4.12) accounts for 80% to 90% of the computed exact results[6] .

Finally, let us consider the angular distribution and polarization of the scattered intensity for natural incident light. We restrict our consideration to the first few glory rings, where

$$u = \beta(\pi-\theta) \tag{4.13}$$

is not >> 1 . In this region, as a first approximation, we find[27,28]

$$S_1(\beta,\theta) \simeq 2\, S^M(\beta) J_1'(u) + 2\, S^E(\beta) J_1(u)/u \ , \tag{4.14}$$

where J_1 is Bessel's function of the first order; we obtain $-S_2$ by interchanging S^M and S^E. At $\theta = \pi$, this reduces to (4.2). van de Hulst[2,3] had proposed an expression of this form with unknown coefficients c_1 and c_2, corresponding respectively to $2S^M$ and $2S^E$.

The polarized intensities associated with S_1 and S_2 follow from (2.6). For natural incident light, the angular distribution and polarization are proportional, respectively, to i_1+i_2 and to $(i_1-i_2)/(i_1+i_2)$, so that they depend on the relative magnitude and phase of S^M and S^E in (4.14). For large u, S_1 is dominated by S^M and S_2 by S^E, as expected. Inspection of the graphs of $J_1'^2(u)$ and $J_1^2(u)/u^2$ shows[34] that the first dark ring will be hazy when the orders of magnitude of S^M and S^E are comparable. Also, the polarization of the outer rings tends to be mainly perpendicular when S^M predominates and mainly parallel when S^E predominates.

According to (3.4), magnetic polarization is dominant in the 10th-order rainbow contribution, in agreement with Sect. 3,(iii) and with Fig. 7. It follows from (4.10) that electric polarization is dominant in the van de Hulst term; this may also be seen in Fig. 7.

The nature of the leading contribution to the glory changes with β in the range 10^2-10^3; the angular distribution and polarization undergo corresponding changes. In particular, near $\beta \sim 10^2$, where the van de Hulst term predominates, the outer rings tend to be parallel-polarized and the first dark ring is rather hazy (this is the situation in most reported observations of natural glories[3]);

near $\beta \sim 10^3$, the rainbow contribution is dominant and the outer rings tend to be perpendicular-polarized (feature (viii)).

5. CONCLUSION

The complex angular momentum theory of Mie scat - tering allows us to account completely for both rainbow and glory effects. In both cases, contributions from dif fracted light appear as a kind of analytic continuation from ray optics, representing the penetration into regions forbidden to real rays. Thus, use of the complex angular momentum theory leads to new insights and allows us to treat a new domain in optics.

The characteristic feature of rainbow scattering is the coalescence of real rays that become complex; this allows us to separate it from other interfering contribu tions that emerge in the same direction. We obtain a uniform asymptotic expansion for a rainbow contribution of arbitrary order. The Airy theory represents a crude approximation to this expression, which already fails bad ly for parallel polarization in the primary bow, and for both polarizations in higher-order bows. The domain of applicability of the complex angular momentum theory also extends to much lower values of β .

The glory arises from incident rays in the edge domain (2.13). After penetrating inside the sphere close to the critical angle, they are almost totally reflected (not quite, because of surface curvature), so that orbits

involving many shortcuts through the sphere still contribute appreciably ("orbiting").

While geometrical-optic paraxial-ray contributions are of only marginal importance, non-paraxial contributions to near-backwards scattering, in particular those from the edge domain, are enhanced by axial focusing. Cross-polarization effects are also significant.

The leading contributions to the glory come from the complex domain. Those of surface-wave type, such as the van de Hulst term, are associated with Regge-Debye poles. As a limiting case, one may have higher-order glory rays (such as p=24 for N given by (4.6)), whose contributions are of Fock type. Complex rays within the shadow of higher-order rainbows formed near the backward direction, specially the tenth-order rainbow, represent the other type of leading contribution.

The quasi-periodic features of the glory as a function of size parameter correspond to the existence of closed or nearly-closed orbits, which give rise to narrow spikes through geometrical resonance effects.

Several types of damping with different β-dependence play a role in the glory: the radiation damping of surface waves, the damping of complex-ray rainbow contributions by "tunneling", which is also affected by the broadening of the main rainbow peak as the order of the rainbow increases, and the damping due to multiple internal reflections, which affects both types of contributions.

The nature and the ordering of the leading Debye contributions changes with β due to the competition

among these various damping effects, producing changes in the angular distribution and polarization of the glory. The same effects are responsible for the peak in the average backscattering phase function around $\beta \sim 10^3$.

Quasi-periodic intensity fluctuations with size parameter, similar to those in the glory, also occur at other angles, but their amplitude decreases rapidly as one moves away from the backward direction[20], due to the absence of axial focusing. Their treatment is analogous to that of the glory.

In particular, they give rise to the "ripple" in the extinction efficiency[35] and in the radiation pressure; the latter has been observed[36] by optical-levitation techniques.

The average efficiency factors over a range of size parameters (where the "ripple" component is averaged out), including both extinction and absorption, play an important role in meteorological optics. The complex angular momentum theory of Mie scattering remains valid for complex refractive indices, and it leads to asymptotic expressions for the average efficiency factors[37] that are accurate over a wide range of size parameters and absorptive parts of the complex refractive index[38].

ACKNOWLEDGMENTS

The author wishes to thank Professor Alistair B. Fraser for making available the color photographs of the rainbow and the glory reproduced in Fig. 2 and Fig. 5.

References and Footnotes

[1] A.Sommerfeld, Optics (Academic Press, New York, 1954), p. 247.

[2] H.C.van de Hulst, "A theory of the Anti-Coronae", J.Opt. Soc.Am. 37, 16-22(1947).

[3] H.C.van de Hulst, Light Scattering by Small Particles (Wiley, New York, 1957).

[4] G.Mie, "Beiträge zur Optik trüber Medien, speziell kolloidaler Metallösungen", Ann.Phys. (Leipzig)25, 377-445(1908).

[5] H.C.Bryant and A.J.Cox, "Mie Theory and the Glory", J. Opt.Soc.Am. 56,1529-1532(1966).

[6] S.T.Shipley and J.A.Weinman, "A Numerical Study of Scattering by Large Dielectric Spheres", J.Opt.Soc.Am. 68, 130-134(1978).

[7] N.A.Logan, "Survey of Some Early Studies of the Scattering of Plane Waves by a Sphere", Proc. IEEE 53, 773-785(1965).

[8] W.Franz, Theorie der Beugung Elektromagnetischer Wellen (Springer-Verlag, Berlin,1957).

[9] J.B.Keller, "A Geometrical Theory of Diffraction", in Calculus of Variations and its Applications, Proceedings of Symposia in Applied Mathematics, edited by L.M.Graves (McGraw-Hill, New York,1958), Vol.8.

[10] V.A.Fock, Diffraction of Radio Waves Around the Earth's Surface (Publishers of the USSR Academy of Sciences, Moscow,1946).

[11] B.van der Pol and H.Bremmer, "The Diffraction of Electromagnetic Waves from an Electrical Point Source round a Finitely Conducting Sphere, with Applications to Radio-Telegraphy and the Theory of the Rainbow", Phil.Mag. 24, 141-176, 825-864(1937); 25, 817-837 (1938).

[12] H.M.Nussenzveig, "High-Frequency Scattering by an Impenetrable Sphere", Ann.Phys. (N.Y.) 34, 23-95(1965).

[13] K.W.Ford and J.A.Wheeler, "Semiclassical Description of Scattering", Ann.Phys. (N.Y.) 7, 259-286(1959).

[14] H.M.Nussenzveig, "Applications of Regge Poles to Short-Wavelength Scattering", in Methods and Problems of Theoretical Physics, edited by J.E.Bowcock (North-Holland, Amsterdam,1970), 203-232.

[15] P.J.Debye, "Das Elektromagnetische Feld um Einen Zylinder und die Theorie des Regenbogens", Physik.Z. 9, 775-778(1908).

[16] H.M.Nussenzveig, "High-Frequency Scattering by a Transparent Sphere. I. Direct Reflection and Transmission", J.Math.Phys. 10, 82-124(1969).

[17] M.V.Berry, "Waves and Thom's Theorem", Adv. in Phys. 25, 1-26(1976).

[18] G.B.Airy, "On the Intensity of Light in the Neighborhood of a Caustic", Trans.Camb.Phil.Soc.6, 379(1838).

[19] H.M.Nussenzveig, "The Theory of the Rainbow", Scientific American 236, 116-127(1977).

[20] H.M.Nussenzveig, "High-Frequency Scattering by a Transparent Sphere, II.Theory of the Rainbow and the Glory", J.Math.Phys. 10, 125-176(1969).

[21] V.Khare and H.M.Nussenzveig, "Theory of the Rainbow", Phys.Rev.Lett. 33, 976-980(1974).

[22] C.Chester, B.Friedman and F.Ursell, "An Extension of the Method of Steepest Descents", Proc.Camb.Phil.Soc. 53, 599-611(1957).

[23] For rainbows formed very close to the backward direction, there is an additional enhancement factor of $O(\beta^{1/2})$ due to axial focusing (cf.Sect.4).

[24] The contrary statement in Ref. 19 is an uncalled-for editorial insertion.

[25] J.Bricard, "Contribution à l'Étude des Brouillards Naturels", Ann.Phys. 14, 148-236(1940).

[26] J.D.Walker, "Multiple Rainbows from Single Drops of Water and Other Liquids", Am.J.Phys. 44, 421-433(1976).

[27] V.Khare, "Short-Wavelength Scattering of Electromagnetic Waves by a Homogeneous Dielectric Sphere", Ph.D. thesis, University of Rochester(1975).

[28]V.Khare and H.M.Nussenzveig, to be published.

[29]V.Khare and H.M.Nussenzveig, "Theory of the Glory",Phys. Rev.Lett. 38, 1279-1282(1977).

[30]For the early history of the subject, cf. J.M.Pernter and F.M.Exner, Meteorologische Optik (W.Braumüller, Vienna(1910).

[31]T.S.Fahlen and H.C.Bryant, "Optical Back Scattering from Single Water Droplets", J.Opt.Soc.Am. 58, 304--310(1968).

[32]J.V.Dave, "Scattering of Visible Light by Large Water Spheres", Appl.Opt. 8, 155-164(1969).

[33]M.J.Saunders, "Near-Field Backscattering Measurements from a Microscopic Water Droplet", J.Opt.Soc.Am. 60, 1359-1365(1970).

[34]V.Khare and H.M.Nussenzveig, "The Theory of the Glory", in Statistical Mechanics and Statistical Methods in Theory and Application, edited by U.Landman (Plenum Publishing Corporation, New York, 1977), 723-764.

[35]P.Walstra, "Light Scattering by Dielectric Spheres:Data on the Ripple in the Extinction Curve", Proc.Koninkl. Nederl.Akad.Wetensch. B67, 491-499(1964).

[36]A.Ashkin and J.M.Dziedzic, "Observation of Resonances in the Radiation Pressure on Dielectric Spheres", Phys.Rev.Lett. 38, 1351-1354(1977).

[37]H.M.Nussenzveig, to be published.

[38]H.M.Nussenzveig and W.J.Wiscombe, to be published.

Figure Captions

FIG.1. Tangential incident ray IT gives rise to surface wave along TA, critically refracted to the inside at A, "totally" reflected at B and critically refracted to the outside at C, travelling as surface wave along CT' and reemerging tangentially as the scattered ray T'S. This path with two shorcuts contributes to the p = 2 Debye term.

FIG.2. The primary and secondary bows. Alexander's dark band is the darker region in the sky between the bows. The supernumerary arcs are the narrow arcs visible on the inner side of the primary bow (photograph courtesy of Prof. Alistair B.Fraser).

FIG.3. As θ approaches θ_R from the lit side, the two real saddle points $\bar{\lambda}$'and $\bar{\lambda}$" move towards confluence; for θ in the dark side, they separate along complex conjugate directions.

FIG.4. Comparison between the exact Mie solution for $|S_2 - S_{2,0}|^2$ (———), the intensity $|S_{2,2}^{(R)}|^2$ of the rainbow term according to complex angular momentum theory (----) and the Airy approximation (—•—•—), for N=1.33 and β=1500.

FIG.5. The glory (photograph courtesy of Prof. Alistair B. Fraser).

FIG.6. The closed orbit associated with tangential incidence for $N \approx 1.33007$. The numbers are the values of p

at the vertices. The directions of the adjoining arrows are those of the angles ζ_p defined by (4.7) and (4.9). Their lengths give a qualitative indication of the ordering of surface-wave contributions (-----) by increasing ζ_p and of rainbow contributions (———) by increasing $\varepsilon_{R,p}/p$ (cf. (4.8)). The rainbow angles $\theta_{R,p}$ are shifted from the corresponding ζ_p (this is indicated for $\theta_{R,11}$). This ordering does not take into account reflection damping, which suppresses high-p contributions.

FIG.7. Contributions to $|S^M(\beta)|^2$ and to $|S^E(\beta)|^2$ from Debye terms of various orders p (the values of p are indicated) for $N \approx 1.33007$ and β = 150, 500 and 1500: ——— rainbow terms; ----- surface-wave terms. For β = 150, there are contributions (—•—•—) from values of p that do not appear in Fig.6.

FIG.8. Behavior of $|S^M(\beta)|^2$ for $N \approx 1.33007$ near β=1500: ——— exact; —·——·— approximation by the two leading Debye terms in Fig.7 (p = 11 + p = 24); — — — — approximation by the sum of all Debye terms shown in Fig. 6, without summing over $\Delta p = 48$. The inset shows an amplification (———) of the spike at position A, together with the result obtained by summing over $\Delta p = 48$ (---------).

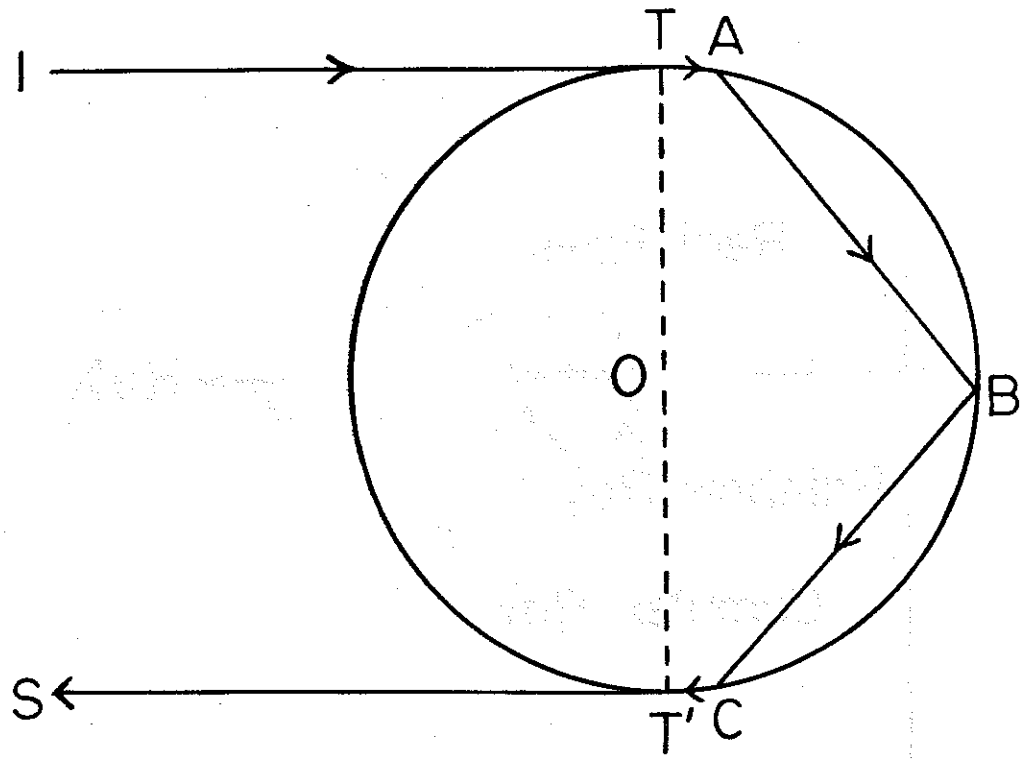

FIG. 1

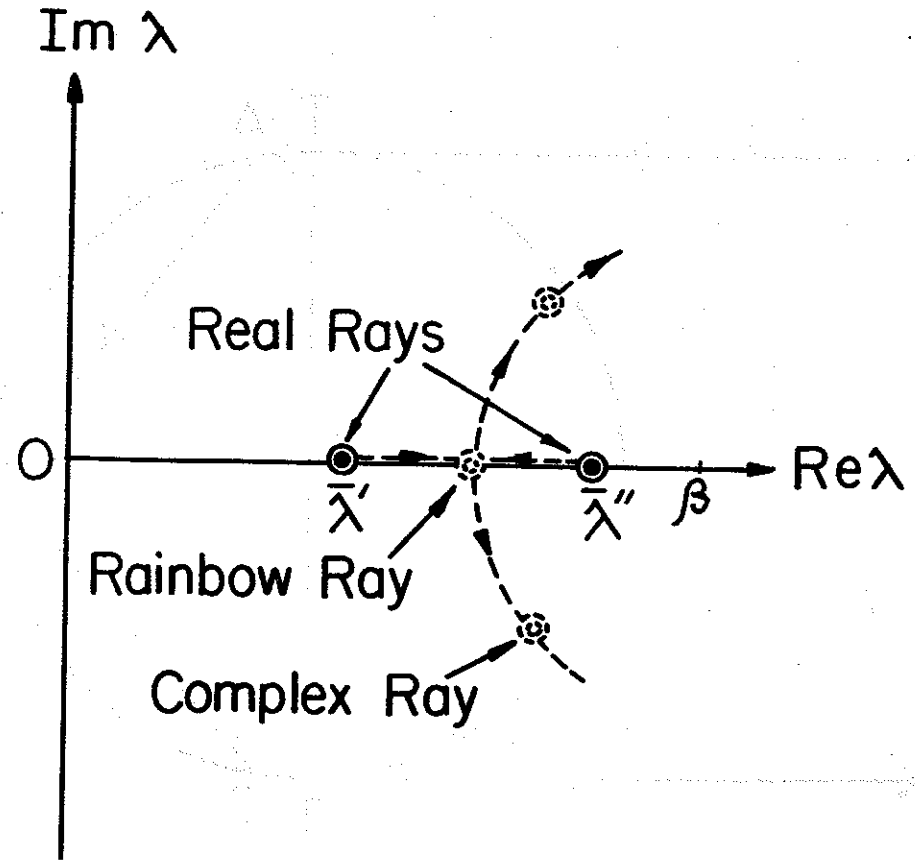

FIG. 3

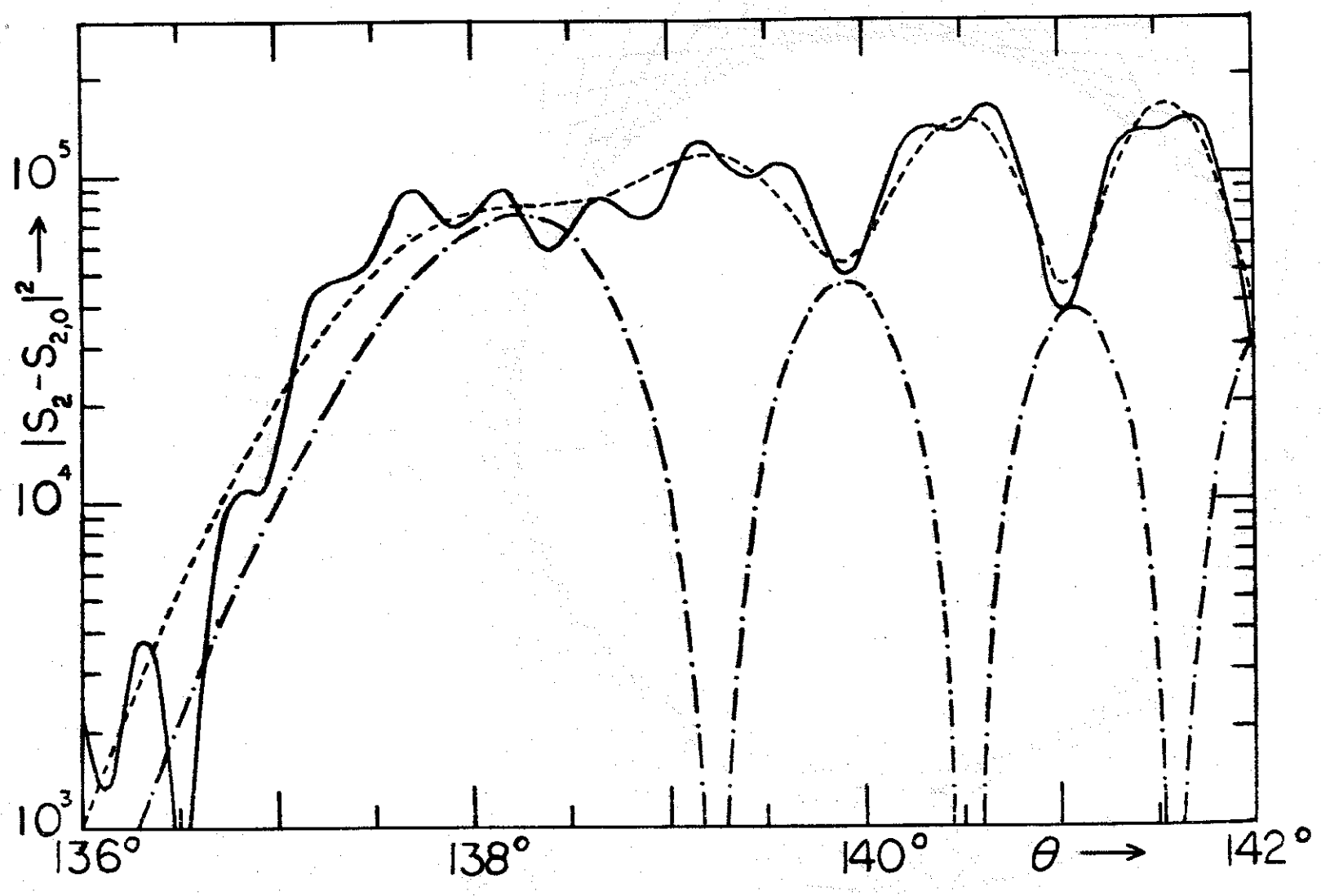
10^5
10^4
10^3
$|S_2 - S_{2,0}|^2 \rightarrow$
136°
138°
140°
$\theta \rightarrow$
142°

FIG. 4

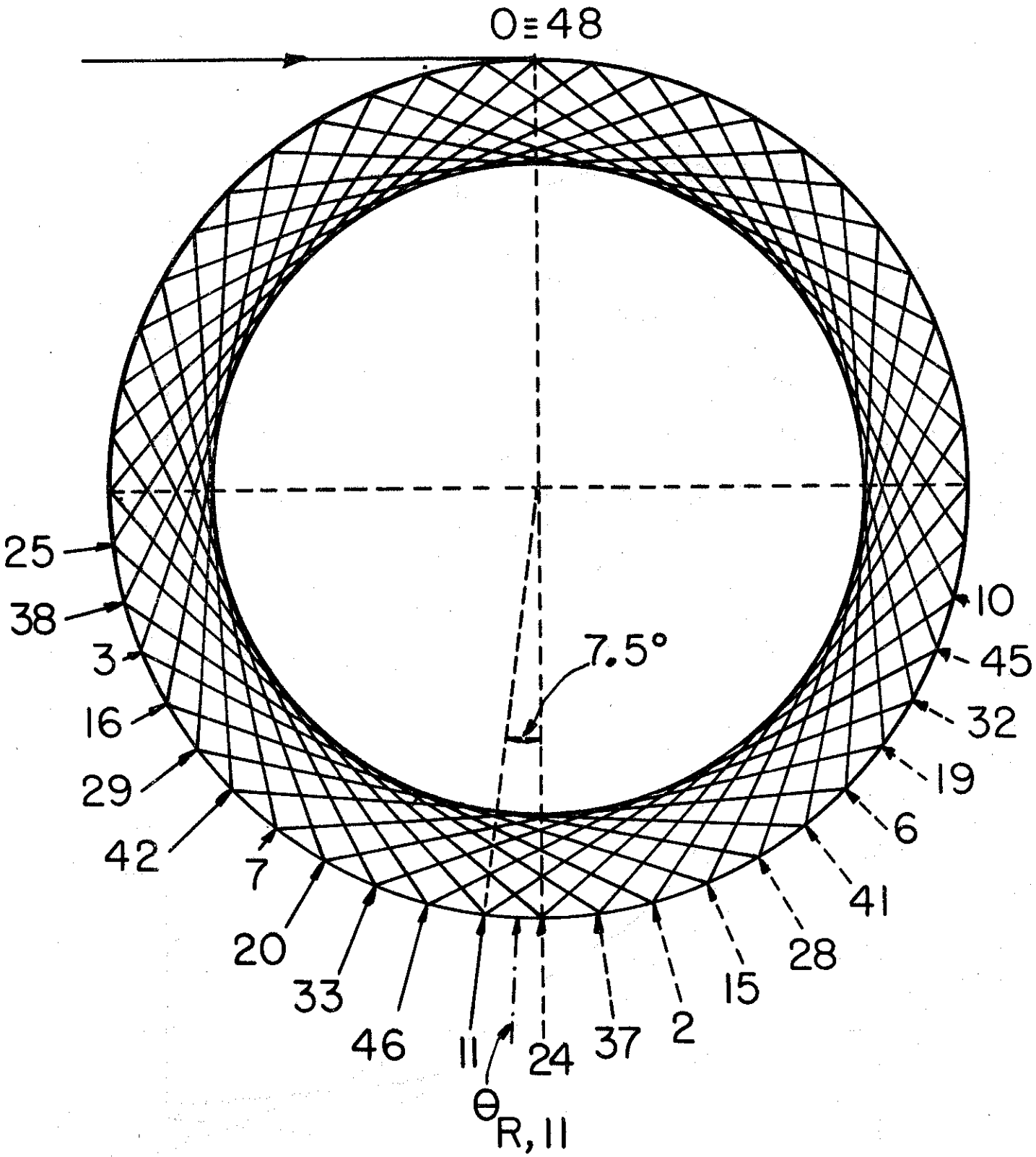
0≡48
25
38
3
16
29
42
7
20
33
46
11
24
37
2
15
28
41
6
19
32
45
10
7.5°
$\theta_{R,11}$

FIG. 6

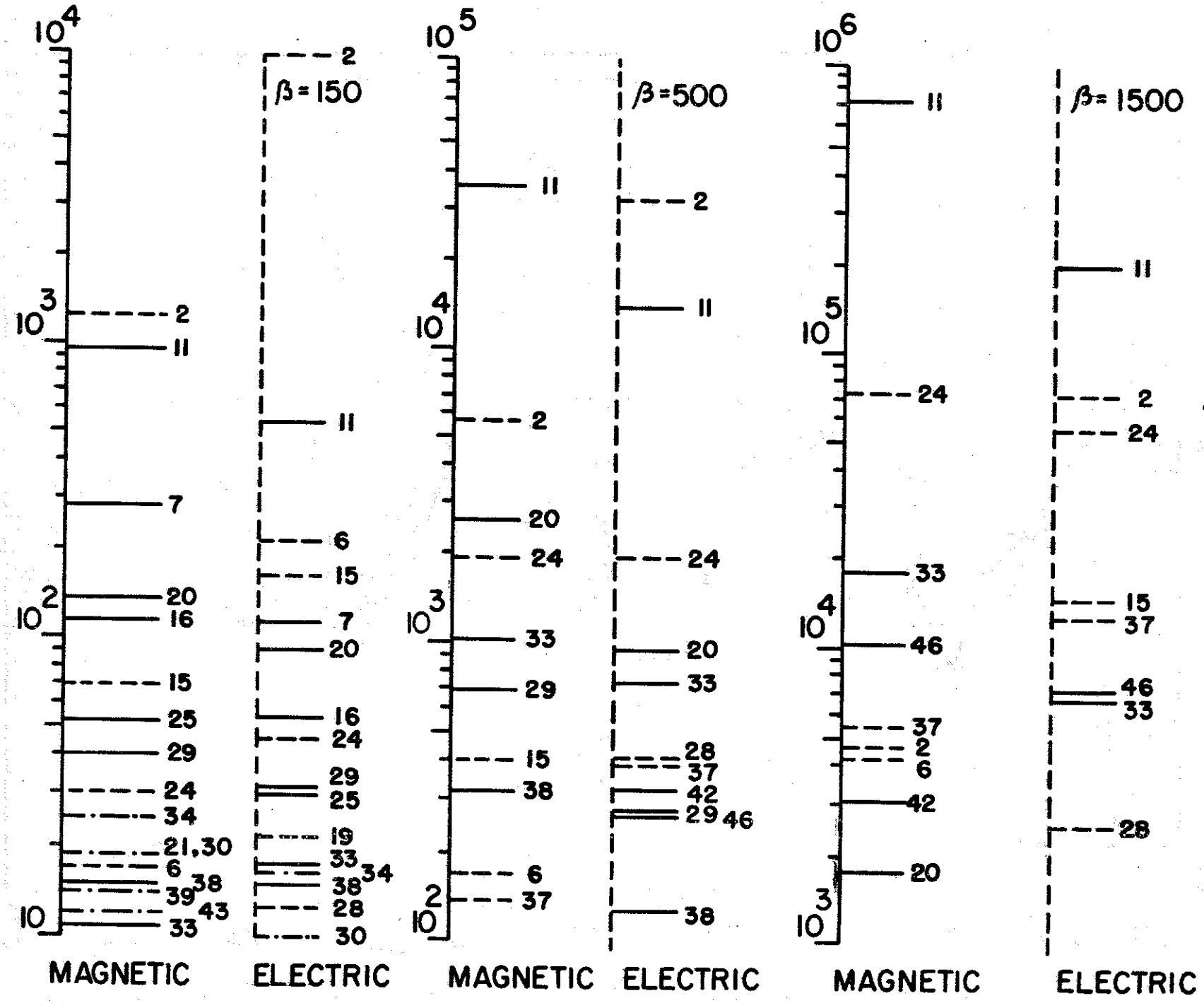
10^4
10^3
10^2
10
2
11
7
20
16
15
25
29
24
34
21,30
6
39
38
43
33
MAGNETIC
$\beta = 150$
2
11
6
15
7
20
16
24
29
25
19
33
34
38
28
30
ELECTRIC
10^5
10^4
10^3
10^2
11
2
20
24
33
29
15
38
6
37
MAGNETIC
$\beta = 500$
2
11
24
20
33
28
37
42
29
46
38
ELECTRIC
10^6
10^5
10^4
10^3
11
24
33
46
37
2
6
42
20
MAGNETIC
$\beta = 1500$
11
2
24
15
37
46
33
28
ELECTRIC

FIG. 7

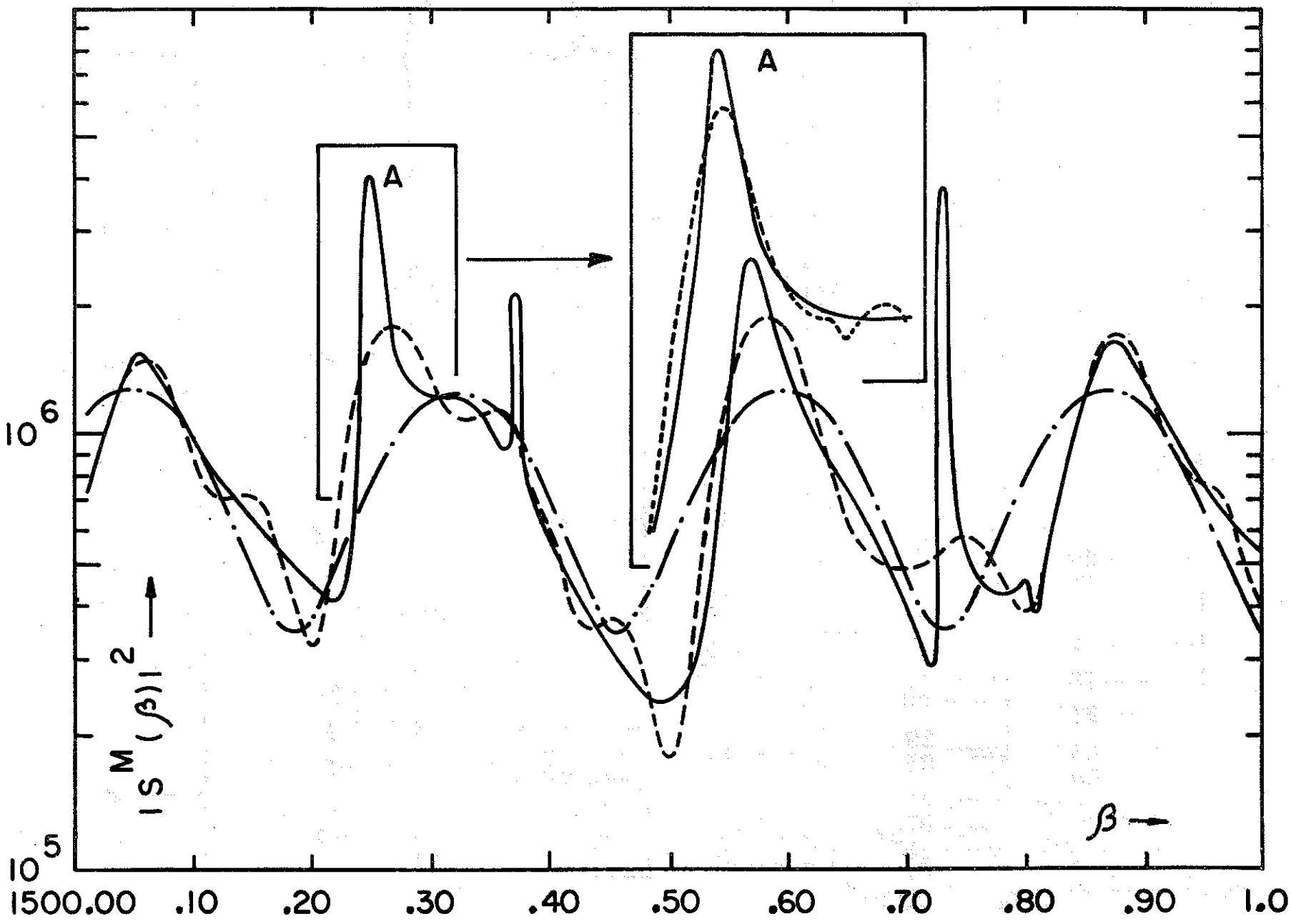

FIG. 8